Electronic structures and ferroelectric instabilities of cubic AV O_3 (A = Sr, Ba, and Pb) perovskites by first-principles calculations

2010 J. Phys.: Condens. Matter 22 125501

(http://iopscience.iop.org/0953-8984/22/12/125501)

J. Phys.: Condens. Matter **22** (2010) 125501 (7pp) doi:10.1088/0953-8984/22/12/125501

Electronic structures and ferroelectric instabilities of cubic AVO_3 (A = Sr, Ba, and Pb) perovskites by first-principles calculations

Shu-yao Yan[1,2], Ying Xie[1], Tao Liu[2] and Hai-tao Yu[1,3]

[1] Key Laboratory of Functional Inorganic Material Chemistry (Heilongjiang University), Ministry of Education, Heilongjiang University, Harbin 150080, People's Republic of China
[2] State Key Laboratory of Theoretical and Computational Chemistry, Institute of Theoretical Chemistry, Jilin University, Changchun 130023, People's Republic of China

E-mail: yuht@scms-hlju.cn

Received 5 November 2009, in final form 25 January 2010
Published 8 March 2010
Online at stacks.iop.org/JPhysCM/22/125501

Abstract
The electronic properties and ferroelectric transition behaviors of three AVO_3 (A = Sr, Ba, and Pb) compounds are investigated by first-principles density functional theory (FP-DFT) in combination with soft-mode theory. The band structures and projection density of states (PDOS) confirm that the bonding properties of $SrVO_3$ and $BaVO_3$ are rather similar to each other, but different to that of $PbVO_3$. The bonding differences determine the ferroelectric transition behaviors of these compounds. For $SrVO_3$ and $BaVO_3$, no ferroelectric instability is observed and they possess cubic structures. The covalent interactions of Pb–O pairs are very important for the ferroelectric instability of $PbVO_3$. In comparison to $PbTiO_3$, we found that the V–O interactions further enhance the ferroelectric instability of $PbVO_3$, and therefore $PbVO_3$ shows a much larger tetragonal distortion than $PbTiO_3$.

(Some figures in this article are in colour only in the electronic version)

1. Introduction

The ABO_3 perovskites are an extremely important group of inorganic materials because of their technological applications and fundamental interests in understanding the nature of phase transitions. Generally, they possess a common high-temperature prototype cubic structure, in which A- and B-site atoms are respectively located at the corner and center of the cubic lattice with O atoms at the face center position. With decreasing temperature, they can exhibit different phase transitions from antiferrodistortive (AFD) to ferroelectric (FE) and antiferroelectric (AFE) phases in nature [1].

Among the family, a series of compounds have been the focus of much experimental and theoretical work for several decades. For example, the structural and electronic properties and transition characteristics of the $ATiO_3$ and $AZrO_3$ (A = Ca, Sr, Ba, and Pb, etc) compounds are clearly elucidated nowadays [2–7]. These perovskites are all insulating and without magnetism. However, as the B-site atoms are substituted by certain magnetic transition metals, the materials are expected to display novel magnetoelectric and multi-ferroic properties, which has attracted renewed attention in recent years [8–12]. Being an important category of perovskite-based oxides, the AVO_3 (A = Sr, Ba, and Pb) compounds are very interesting. In the oxides, V^{4+} is often magnetic and can locate at the centers of octahedral oxygen cages, as in cubic $SrVO_3$ [8, 9]. When the crystal symmetry is reduced from cubic to tetragonal, an unusual metal-to-insulator transformation may be observed [10, 11]. As the A-site atoms are changed, the materials may show different stable phases, resulting in different properties. Due to the above mentioned $3d^1$ electronic configurations, (V^{4+}) and simple crystal structures, the AVO_3 compounds were considered to possess many potential applications in fields such as multi-ferroic devices, high-temperature solid oxide fuel cells, high T_c superconductivity, and so on [8, 12].

[3] Author to whom any correspondence should be addressed.

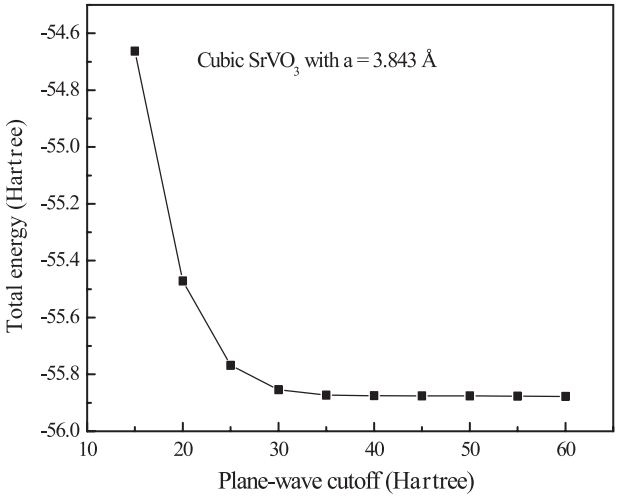

Figure 1. Convergence test for plane-wave basis set.

Despite their potential importance, relevant investigations on the AVO_3 compounds are relatively scarce. Strontium vanadate was the first synthesized AVO_3 compound and reported to have a cubic structure with cell parameter a = 3.840–3.849 Å [8, 13]. Later experiments showed that its electric resistivity is rather small and no higher than 50 mΩ cm in the temperature range from 0 to 300 K [8]. By using the local density approximation and dynamical mean-field theory (LDA-DMFT), Nekrasov and co-workers have calculated the band structures and density of states (DOS) of cubic $SrVO_3$, and their results are in agreement with bulk-sensitive photoemission and x-ray absorption experiments [9]. Quite recently, with the application of high-temperature and high-pressure techniques, $PbVO_3$ was successfully synthesized for the first time [10]. This compound was found to possess a very large tetragonal distortion (c/a, 1.23) [10, 11]. The temperature-dependent XRD data indicated that the tetragonal to cubic phase (T-to-C, ferroelectric to paraelectric) transition in $PbVO_3$ is above the decomposition temperature [11]. Only at high pressure (about 2 GPa), can the T-to-C phase transition be realized at room temperature [11]. Further theoretical calculations confirm that the T-to-C phase transition has an insulator-to-metal transformation characteristic and the important interactions in $PbVO_3$ originate from the Pb_{6p}–O_{2p} and V_{3d}–O_{2p} states [11, 13]. As for $BaVO_3$, its tolerance factor is very close to that of $BaTiO_3$, and the two compounds may show similar structural and transition properties [14]. However, related investigations on $BaVO_3$ are still absent at present and need further consideration. Furthermore, the substitution of A-site atoms may have distinct effect on the structures of these compounds and hence their properties. Relevant investigations are thus very helpful not only in clarifying the transition behaviors of these compounds but also in elucidating the origin of the largest tetragonality of $PbVO_3$.

With these motivations in mind, the present investigation is aimed at providing an application of first-principles techniques to obtain the electronic structures and distinguish the transition behaviors of these compounds.

Table 1. Theoretical and experimental lattice constants of AVO_3 compounds.

	$a = b = c$ (Å)		
	$SrVO_3$	$PbVO_3$	$BaVO_3$
Present	3.839	3.890	4.059
Experiments	3.843 [8]	3.900 [11]	—
Error	−0.09%	−0.28%	—

2. Computational method

The present calculations were performed by the ABINIT [15, 16] package within the Kohn–Sham formulation of density functional theory [17] using the plane-wave pseudo-potential technique [18]. The local spin density approximation potentials (LSDA) used in the calculations were generated by the Troullier–Martins scheme [19] by the FHI98PP code [20]. The Perdew–Wang 92 functional was applied in the calculation [21]. The electronic wavefunctions were tested and the plane wave with a kinetic cutoff of 35 Hartree was determined, as showed in figure 1. The sampling over the Brillouin Zone was treated by a 4 × 4 × 4 Monkhorst–Pack mesh [22]. To consider the spin effect, we have set up the spin states for every kind of atom in the investigated compounds. As mentioned above, the crystal structure of $BaVO_3$ is still unclear, and therefore geometry optimizations are necessary. For the three cubic crystals, the total energy dependence of the lattice constants was calculated using single-point techniques and the equilibrium lattices were determined by the fitted singlet-point potential energy curves. In all calculations, the total energy difference between two iterations is restricted to 10^{-7} eV to ensure a good precision. Table 1 lists the theoretical and experimental lattice constants of the three compounds. It can be noted from table 1 that the maximum error is only 0.28%, indicating a satisfactory agreement with experimental results.

As the phase transitions of ABO_3 perovskites usually follow the sequence from high to low symmetry, in the present calculation we mainly consider the ferroelectric instability and transition possibilities of cubic structures. Moreover, in the structures, the Sr (Ba and Pb), V, and O atoms are located at the corner, center and face center positions of the cubic lattice, respectively.

3. Results and discussion

3.1. Electronic structure

To clarify the structural and electronic property differences, the band structure, density of states (DOS), and electron density were investigated. Figure 2 shows the majority and minority spin bands. The Fermi energies were computed to be −4.25, −5.14, and 0.17 eV for $SrVO_3$, $BaVO_3$, and $PbVO_3$, respectively. It can be noted that, in the order of increasing energy, the band of $SrVO_3$ consists of nine O_{2p} derived bands, which are three-fold degenerate at the Γ point of the Brillouin zone, and then separated by a energy gap, a

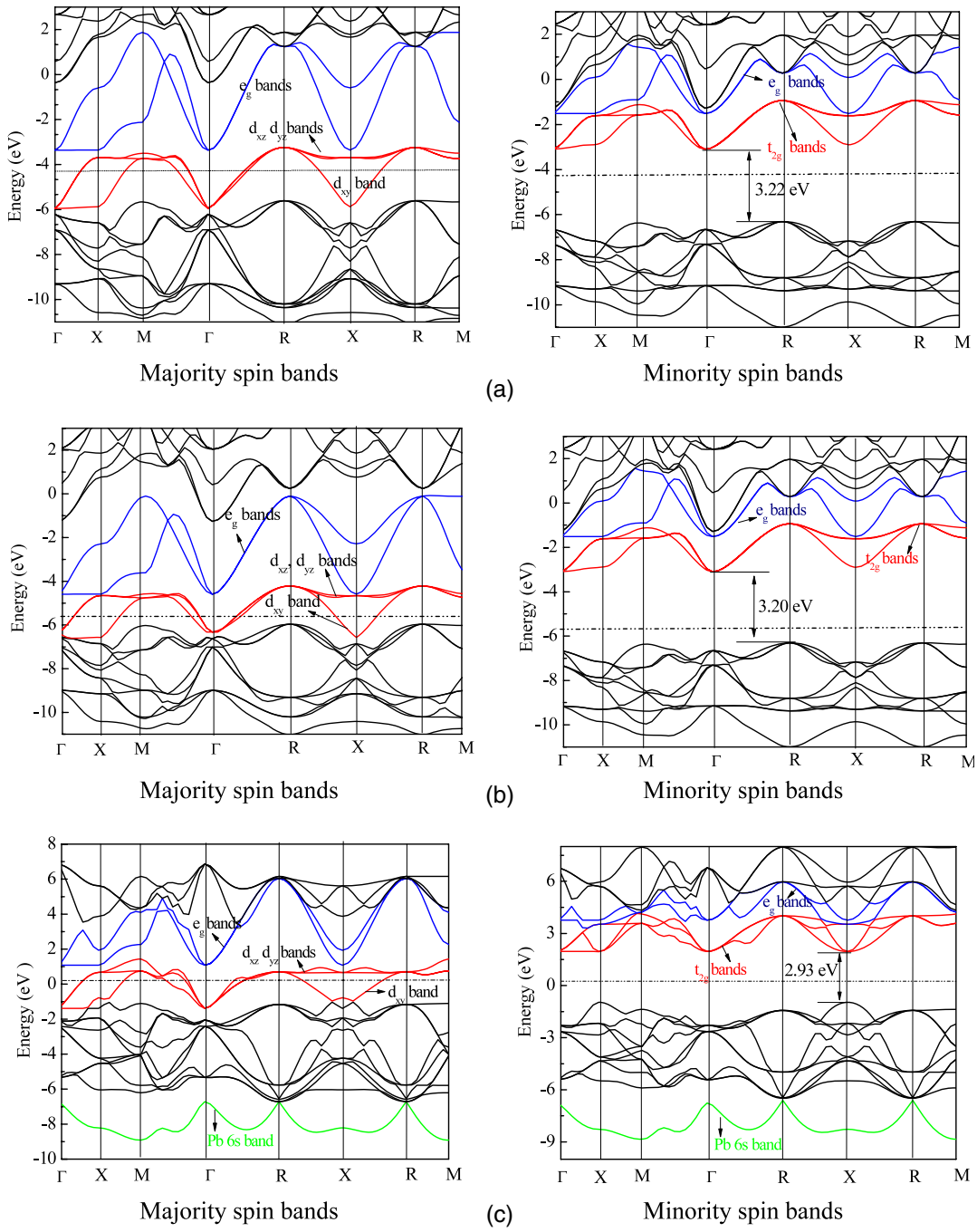

Figure 2. Majority (left) and minority (right) spin bands for (a) $SrVO_3$, (b) $BaVO_3$, and (c) $PbVO_3$. The red and blue lines represent the V_{3d}–t_{2g} and V_{3d}–e_{2g} states respectively, while the green line represents the Pb_{6s} band. The dashed lines indicate the position of the Fermi energy.

manifold of V_{3d} derived bands are observed. The energy bands at higher energy positions (above 0.0 eV) can be attributed to Sr_{5s} and Sr_{5p} states. Figure 3(a) shows the projections of the DOS onto different atoms. According to the decomposition, it can be clearly confirmed that hybridization between the V_{3d} and O_{2p} states is dominant in $SrVO_3$, while the relative small contributions from Sr_{5s} and Sr_{5p} states to the valence bands ([−12 eV, −6 eV]) indicate that Sr possesses highly ionic characteristics. Due to the octahedral crystal fields (V–O octahedron), the V_{3d} levels are split into two groups, namely the lower lying t_{2g} and higher lying e_g bands. Since the O_{2p} bands lie below the V_{3d} bands, the V_{3d} orbitals are formally anti-bonding. The stronger the interactions between the V_{3d} and O_{2p} states, the higher the energy position of the V 3d bands is pushed. According to the minority spin bands of $SrVO_3$, it can be known that the V_{3d} bands lie 3.22 eV above the O_{2p} ones. Moreover, the band structure of $SrVO_3$ also shows that the V_{3d}–t_{2g} bands are further split into a lower d_{xy} band and a higher two-fold degenerated d_{xz} and d_{yz} group. The above peculiar splitting explains the multi-peak features of the V_{3d} DOS very well. In the case of V^{4+}, there is one d electron filled in the d_{xy} orbital, which forms local moments

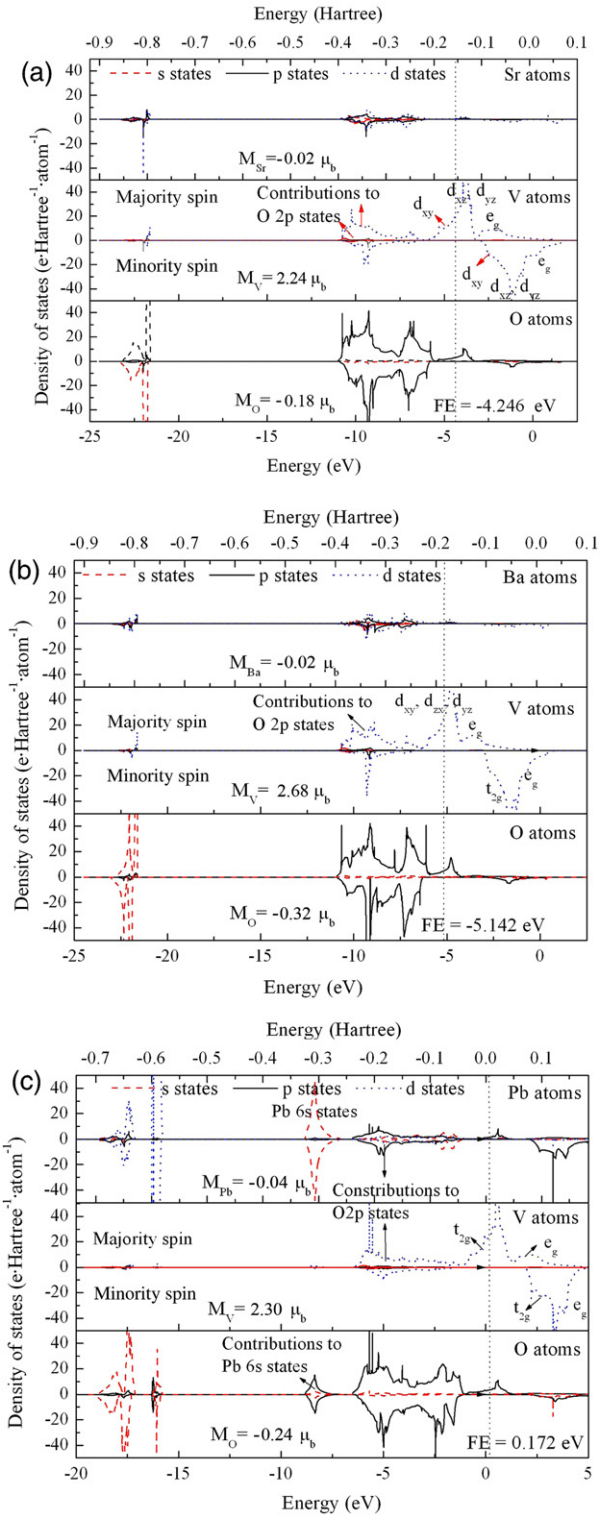

Figure 3. Projection density of states (PDOS) of different atoms for (a) $SrVO_3$, (b) $BaVO_3$, and (c) $PbVO_3$. Positive and negative values mean majority and minority spins respectively. Two measurement units are used on the X-axis, Hartree on the top and eV on the bottom. The magnetizations of atoms (M, in Bohr magneton (μ_b)) are also given.

due to the Hund coupling. Therefore, the system shows a half-metallic characteristic. The computed band structure of $SrVO_3$ is consistent with previous LDA-DMFT results [9]. Furthermore, we also calculated the magnetization of the three compounds based on the equation

$$M = g_e \mu_b \left(\int_{-\infty}^{EF} n_\uparrow(E)\,dE - \int_{-\infty}^{EF} n_\downarrow(E)\,dE \right)$$

in which g_e and μ_b are the spin factor and Bohr magneton, respectively. The computed results are listed in figure 3.

Figures 2(b) and 3(b) depict the band structure and projection DOS of $BaVO_3$. The results clearly show that the A–O and V–O bondings of $BaVO_3$ are almost identical to that of $SrVO_3$, and the substitution of Sr by Ba does not significantly affect the covalent nature of the compounds. According to previous investigations, the bonding between two atoms can be decomposed into two parts, namely the long-range Coulomb interactions and short-range repulsions [5, 23]. For $ATiO_3$ and $AZrO_3$ (A = Sr, Ba, and Pb) perovskites, the long-range Coulomb characteristics of the A–O pair are crucial for the antiferrodistortive behavior of the compounds, while those of the B–O pair account for the ferroelectric instability [5, 23]. The very similar covalent bondings in $SrVO_3$ and $BaVO_3$ suggest that the long-range interactions of A–O and B–O pairs are similar to each other. As already confirmed in our previous investigations on $SrTiO_3$ and $BaTiO_3$, the long-range interactions of A–O and B–O pairs are rather close in the two compounds with the same lattice volume, while the short-range repulsions of the two pairs related to the ion radius are indeed very different [23]. The larger the ion radius, the stronger the repulsions of corresponding pairs. For $BaTiO_3$, the large ion radius of Ba results in a larger lattice volume, which is very crucial for its ferroelectric instability [23]. As a result, $BaTiO_3$ undergoes a ferroelectric phase transition, which is absent in $SrTiO_3$ [23, 24]. For $BaVO_3$ and $SrVO_3$, a similar effect exists, and the repulsions between A and O atoms are expected to be larger in $BaVO_3$. Therefore, the lattice constants of $BaVO_3$ should be larger than those of $SrVO_3$, which can be demonstrated by the results listed in table 1 ($BaVO_3$ is 5.7% larger than $SrVO_3$). However, to confirm whether the larger lattice volume of $BaVO_3$ can result in possible ferroelectric instability and transitions, further calculations are needed. These will be performed in section 3.2.

Figures 2(c) and 3(c) show the band structure and projection DOS of $PbVO_3$. In comparison to $SrVO_3$ and $BaVO_3$, the bonding properties of $PbVO_3$ change significantly. The energy band located at about −7.5 eV is attributed to the Pb 6s state, and its splitting indicates a covalent interaction between Pb 6s and O 2p states, being consistent with the resonance peak features shown in the projection DOS. This particular bonding is very common indeed in Pb-based ABO_3 perovskites and essential for the O atoms in the crystal lattice to deviate from their equilibrium positions along the [001] direction, leading to a larger tetragonal distortions, as found in $PbTiO_3$ and $PbZrO_3$ [5]. Figure 4 depicts the electron density of the [001] crystal plane through different atoms. For $SrVO_3$ and $BaVO_3$, the electrons located at the Sr and Ba atoms are rather scarce, and the electron density overlap between A (A = Sr, Ba) and O atoms is also absent. The result confirms that Sr and Ba are highly ionic and no covalent bonds are formed between A and O atoms. On the contrary, the situation in

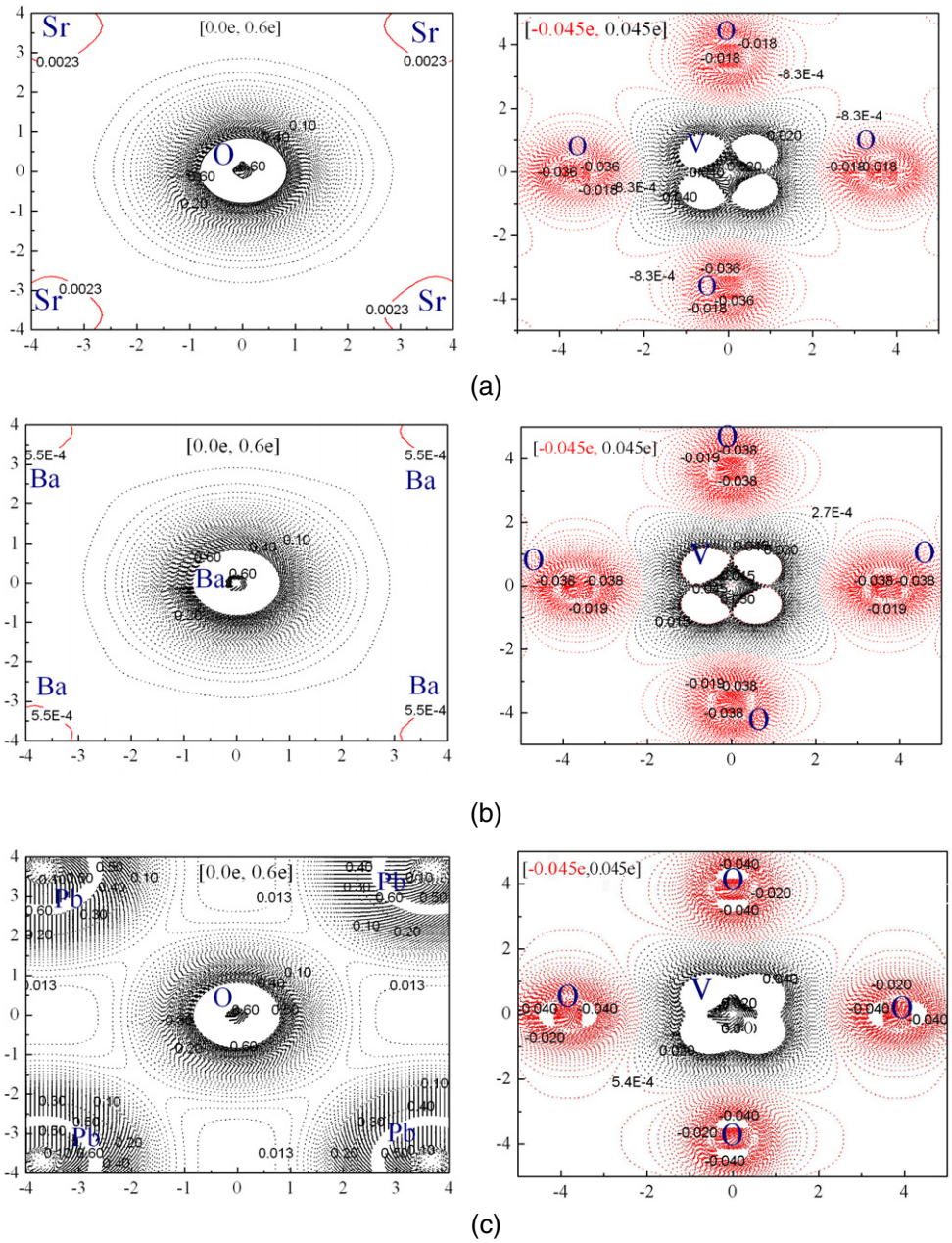

Figure 4. Electron density diagram of the (001) plane for (a) $SrVO_3$, (b) $BaVO_3$, and (c) $PbVO_3$. The left panel shows the total electron density through the A and O atomic plane, while the right panel depicts the electron density differences through the V and O plane.

$PbVO_3$ is rather different. The electrons located in the Pb 6s states not only result in significant electron distributions at the Pb site but also an electron density overlap between Pb and O atoms, confirming the covalent characteristics of the Pb–O bonds. For the presently investigated AVO_3 compounds (A = Sr, Ba, Pb), the electron density difference diagram (right panel of figure 4) clearly shows that V_{3d} states lose electrons (in black) while O_{2p} states (in red) gain electrons, and the V_{3d} states strongly hybridize with the O_{2p} states. The electron density again confirms the A–O and B–O bonding characteristics discussed above. As the bonding of the systems is crucial for the transition behavior and the ferroelectric instabilities are mainly connected to the displacement potential energy surface (PES) of the center transition metal atoms, in the next section the energy changes as a function of V displacements along the [001] direction are considered.

3.2. Potential energy surface (PES)

According to the soft-mode theory, the phase transitions of materials are related to the congelation of soft phonons [1]. Usually, the ferroelectric soft polar mode of ABO_3 perovskites contains the opposite movements of B atoms against O atoms along the [001] direction, as exemplified in figure 5(e). To explain the congelation process, the total energy dependence of atomic displacements along the soft-mode eigenvector, which is usually called the potential energy surface [2] or potential energy curve, is applied in the present calculations. For

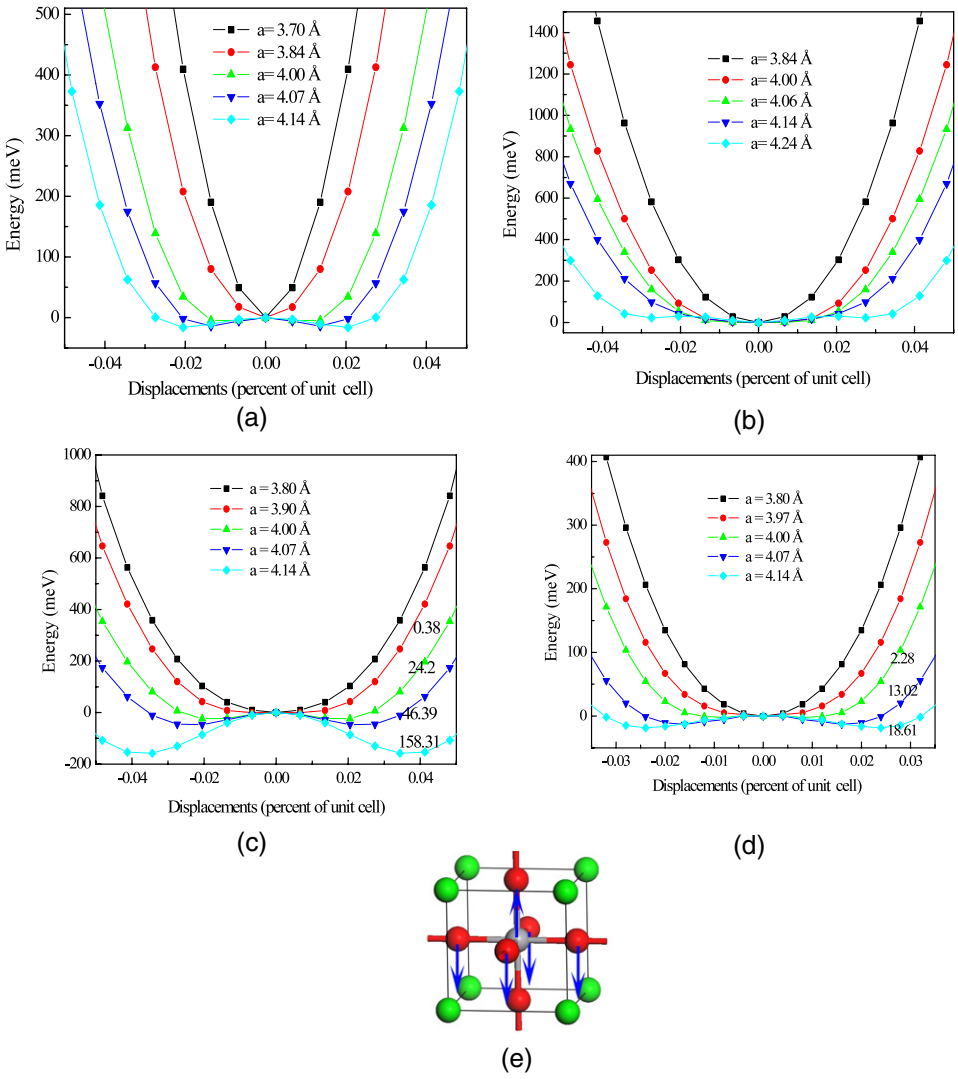

Figure 5. Potential energy surfaces of V and Ti atoms as a function of lattice volume for cubic (a) $SrVO_3$, (b) $BaVO_3$, (c) $PbVO_3$, and (d) $PbTiO_3$. Figure (e) shows the eigenvector of the ferroelectric soft mode. The energy zero points are taken from the total energies of corresponding equilibrium configuration.

$SrVO_3$, it can be noted that the atomic displacement PES of V atoms along the [001] direction shows typical single well characteristics at the equilibrium lattice constant. Therefore, the V atoms can not deviate from their equilibrium position as the temperature is lowered, and the ferroelectric instability is thus absent in the cubic phase of $SrVO_3$, similar to the behavior of $SrTiO_3$ [23, 24]. The result can be further confirmed by the calculated lowest frequency optical phonon at the Gamma point of the equilibrium lattice, i.e. 144.8 cm^{-1}, 125.1 cm^{-1}, and -71.2 cm^{-1} for $SrVO_3$, $BaVO_3$ and $PbVO_3$ respectively. However, as the lattice volume is expanded by 7.8%, a double well with a depth of 16.09 meV can be obtained, suggesting that the cubic $SrVO_3$ may show ferroelectric instability at high vacuum or negative pressure conditions. Figure 5(b) shows the computation results for $BaVO_3$. In consideration of the bonding similarity and structural differences aforementioned, $BaVO_3$ is expected to possess some ferroelectric instability because of its larger lattice constant. However, the results clearly indicate that all the curves obtained under different lattice constants possess single well characteristics, and the cubic phase of $BaVO_3$ lacks any ferroelectric instability. The results are different from those observed in $SrTiO_3$ and $BaTiO_3$, in which the ferroelectric transition behaviors can be distinguished by the lattice volume and radius of Ba [23].

Figure 5(c) depicts the results for $PbVO_3$. Due to the Pb–O covalent interactions, the O atoms tend to displace away from their equilibrium positions, and opposite displacements between O and V atoms thus occur. The displacement PES of the V atoms thus shows a double well characteristic in the equilibrium lattice. According to the soft-mode theory, when the temperature drops below a certain Curie point, the V atoms are trapped at the energy minimum and, therefore, macropolarization along the [001] direction appears, leading to the occurrence of a ferroelectric phase transition. It should be emphasized that the deeper the well depth, the stronger the ferroelectric instability, and the lower the transition temperatures observed. In comparison to $PbVO_3$, the well depths of Ti atoms in $PbTiO_3$ (figure 5(d)) are much smaller at the same lattice constant. This result explains well the fact that $PbTiO_3$ undergoes a ferroelectric transition from the

paraelectric cubic phase to the ferroelectric tetragonal phase at 766 K [2], while the temperature of the corresponding transition for $PbVO_3$ is above the decomposition temperature and cannot be observed in experiment [11]. Moreover, it can be found that the well depth of V atoms in $PbVO_3$ decreases gradually when the lattice constant is suppressed. As a result, the ferroelectric instability of $PbVO_3$ is weakened and the tetragonal to cubic transition becomes available under pressure, being consistent with the experimental observations that the transition appears at about 2 GPa at room temperature [11]. Despite the well depth, the V displacements of $PbVO_3$ are also found to be larger than the Ti displacement of $PbTiO_3$, which results in a larger tetragonal distortion of $PbVO_3$ (1.23) than that of $PbTiO_3$ (1.06) [2]. By comparison of the crystal structures, it can be clarified that the different behaviors of $PbVO_3$ and $PbTiO_3$ are mainly due to the B–O (B = Ti and V) interactions. Although the decomposition of the B–O interaction is absent at present, however, the calculations have at least confirmed that the smaller ion radius of V with respect to Ti is not only helpful for reducing the lattice constant but also weakens the short-range repulsions of the V–O pairs, leading to a very large tetragonal distortion for $PbVO_3$.

4. Conclusions

Relying on first-principles density functional theory, the band structures, density of states, and electron density of three AVO_3 (A = Sr, Ba, and Pb) compounds were calculated. The computational results indicated that $SrVO_3$ and $BaVO_3$ have very similar bonding characteristics. Sr and Ba atoms are both highly ionic, and the V atoms strongly bonded to O atoms. For $PbVO_3$, the covalent interactions between Pb and O atoms, which are different in $SrVO_3$ and $BaVO_3$, result in different transition behaviors. The results from PES indicate that no ferroelectric instabilities can be found in $SrVO_3$ and $BaVO_3$. For $PbVO_3$, the smaller radius of V with respect to Ti reduces the lattice constant and weakens the V–O repulsions. Therefore, the ferroelectric instability of $PbVO_3$ is much stronger than that of $PbTiO_3$, explaining well the much larger tetragonal distortion of $PbVO_3$.

References

[1] Lines M E and Glass A M 1977 *Principles and Applications of Ferroelectrics and Related Materials* (Oxford: Clarendon)
[2] Cohen R E 1992 *Nature* **358** 136
[3] King-Smith R D and Vanderbilt D 1994 *Phys. Rev.* B **49** 5828
[4] Zhong W and Vanderbilt D 1995 *Phys. Rev. Lett.* **74** 2587
[5] Ghosez Ph, Cockayne E, Waghmare U V and Rabe K M 1999 *Phys. Rev.* B **60** 836
[6] Piskunov S, Heifets E, Eglitis R I and Borstel G 2004 *Comput. Mater. Sci.* **29** 165
[7] Chen Z X, Chen Y and Jiang Y S 2002 *J. Phys. Chem.* B **106** 9986
[8] Lan Y C, Chen X L and He M 2003 *J. Alloys Compounds* **354** 95
[9] Nekrasov I A, Held K, Keller G, Kondakov D E, Pruschke Th, Kollar M, Andersen O K and Anisimov V I 2006 *Phys. Rev.* B **73** 155112
[10] Shpanchenko R V, Chernaya V V, Tsirlin A A, Chizhov P S, Sklovsky D E, Antipov E V, Khlybov E P, Pomjakushin V, Balagurov A M, Medvedeva J E, Kaul E E and Geibel C 2004 *Chem. Mater.* **16** 3267
[11] Belik A A, Azuma M, Saito T, Shimakawa Y and Takano M 2005 *Chem. Mater.* **17** 269
[12] Hui S Q and Petric A 2001 *Solid State Ion.* **143** 275
[13] Singh D J 2006 *Phys. Rev.* B **73** 094102
[14] Goudochnikov P and Bell A J 2007 *J. Phys.: Condens. Matter* **19** 176201
[15] Gonze X, Beuken J M, Caracas R, Detraux F, Fuchs M, Rignanese G M, Sindic L, Verstraete M, Zerah G, Jollet F, Torrent M, Roy A, Mikami M, Ghosez Ph, Raty J Y and Allan D C 2002 *Comput. Mater. Sci.* **25** 478
[16] Gonze X, Rignanese G M, Verstraete M, Beuken J M, Pouillon Y, Caracas R, Jollet F, Torrent M, Zerah G, Mikami M, Ghosez Ph, Veithen M, Raty J Y, Olevano V, Bruneval F, Reining L, Godby R, Onida G, Hamman D R and Allan D C 2005 *Z. Kristallogr.* **220** 558
[17] Hohenberg P and Kohn W 1964 *Phys. Rev.* **136** A864
Kohn W and Sham L J 1965 *Phys. Rev.* **140** A1133
[18] Vanderbilt D 1990 *Phys. Rev.* B **41** 7892
[19] Troullier N and Martins J L 1991 *Phys. Rev.* B **43** 1993–2006
[20] Fuchs M and Scheffler M 1999 *Comput. Phys. Commun.* **119** 67
[21] Perdew J P and Wang Y 1992 *Phys. Rev.* B **45** 13244
[22] Monkhorst H J and Pack J D 1976 *Phys. Rev.* B **13** 5188
[23] Xie Y, Yu H T, Zhang G X and Fu H G 2008 *J. Phys.: Condens. Matter* **20** 215215
[24] Trautmann T and Falter C 2004 *J. Phys.: Condens. Matter* **16** 5955